PROCEEDINGS OF SCIENCE

Selecting stopping muons with KM3NeT/ORCA

Louis Bailly-Salins[a,*] **on behalf of the KM3NeT collaboration**

[a] *Université de Caen Normandie, ENSICAEN, CNRS/IN2P3, LPC Caen UMR 6534, F-14000 Caen, France*

E-mail: baillysalins@lpccaen.in2p3.fr

The KM3NeT collaboration operates two water Cherenkov neutrino telescopes in the Mediterranean sea, ORCA and ARCA. The flux of atmospheric muons produced in cosmic ray air showers forms a background to the main objectives of KM3NeT/ORCA and KM3NeT/ARCA, respectively measuring atmospheric neutrino oscillations and detecting neutrinos from astrophysical sources. A small portion of the atmospheric muons stops inside the detector's instrumented volume. The stopping muons are 5% of the muons reconstructed using the 6 first strings deployed for ORCA. This still amounts to 1000 events per hour. We present two methods for selecting them, applied on both simulations and data. The first method uses simple cuts on a set of reconstructed variables. The second method uses a machine learning model to classify muons as "stopping" or "crossing". Both methods allow to reach a high selection purity, close to 95%. Detecting stopping muons can serve many purposes like studying muon decay via the detection of Michel electrons or estimating the flux of atmospheric muons at sea level. This work highlights the accurate reconstruction capabilities of ORCA. The median error on the reconstructed stopping point of selected muons is less than 5 meters, and the median angular deviation is 1°. This is to be compared with the 20 meters horizontal distance between strings and the 9 meters vertical distance between optical modules. Another important result is the excellent agreement between distribution of stopping muons selected in data and in simulations.

38th International Cosmic Ray Conference (ICRC2023)
26 July - 3 August, 2023
Nagoya, Japan

*Speaker

PoS(ICRC2023)203

1. Introduction

The KM3NeT collaboration operates two water Cherenkov neutrino telescopes in the Mediterranean sea [1]. ORCA (*Oscillation Research with Cosmics in the Abyss*), at a depth of 2450 m, is designed to measure atmospheric neutrinos oscillations. ARCA (*Astroparticle Research with Cosmics in the Abyss*), at a depth of 3450 m, is designed to detect neutrinos from astrophysical sources. ARCA and ORCA share the same technology and detector elements. Both detectors are instrumented with photomultiplier tubes (PMTs) for the detection of Cherenkov light emitted along the path of the relativistic charged particles produced in neutrino interactions. KM3NeT detectors consist of a 3-D array of glass-spheres named Digital Optical Modules (DOMs) [2] housing 31 3-inch PMTs each. The DOMs are arranged along vertical lines called Detection Units (DU) carrying 18 DOMs each. Each DU is anchored to the seabed and remains vertical due to the buoyancy of the DOMs and of a buoy tied on its top. When completed, each detector "building block" will consist of 115 detection units arranged side by side following a cylindrical footprint. The vertical distance between DOMs and horizontal distance between DUs are different for the two detectors. ARCA is optimised to maximise its detection efficiency in the energy range 1 TeV-10 PeV, while ORCA has a denser PMT configuration to detect neutrinos in the range 1-100 GeV.

For both detectors, the vast majority of recorded events does not come from neutrinos but from atmospheric muons produced in cosmic ray air showers. Being deep underwater, the KM3NeT detectors have access to high-energy atmospheric muons [3]. Among the detected atmospheric muons, only a small portion stops inside the instrumented volume. For instance, the stopping muons are 5% of all the muons reconstructed using the 6 first strings deployed for ORCA (this partial configuration is identified in the following as ORCA6). This still amounts to more than 1000 events per hour, offering enough statistics for various purposes. First, the subsequent decay of stopping muons can be studied via the detection of Michel electrons. In addition, stopping muons can be used for tuning parameters related to the light output of the muon tracks in the simulations. Finally, reconstructing the direction and stopping point of a muon track allows to compute the range the particle has crossed through sea water, and thus to estimate the energy it had at sea level. Consequently, selecting stopping muons can lead to a measurement of the atmospheric muon flux at sea level on a given range of energy and direction (around 1 TeV for vertical muons). Given the high uncertainties in the modelling of cosmic ray-induced particle showers [4][5], specifically in the primary cosmic ray flux composition and in the hadronic interaction models, such model-independent measurement would be invaluable.

The first step to this measurement of the atmospheric muons flux at sea level with KM3NeT is to accurately select the muons stopping in the detector. This is what this contribution will describe for the ORCA6 detector.

2. Stopping muons in the KM3NeT detector

Of the two telescopes, ORCA is the one most suited for detecting stopping muons as it is more densely instrumented. The vertical distance between DOMs is around 9 m, and the horizontal distance between DUs is around 20 m. In the following, a stopping muon is defined as *a muon which stops inside the detector's instrumented volume*. As KM3NeT detectors do not have strict

outer boundaries, there is some subjectivity in the definition of the instrumented volume. To stick to pre-existing conventions inside the collaboration, the instrumented volume is defined as *the smallest cylinder containing all the DUs*. Its limits are shown for ORCA6 on Figure 1.

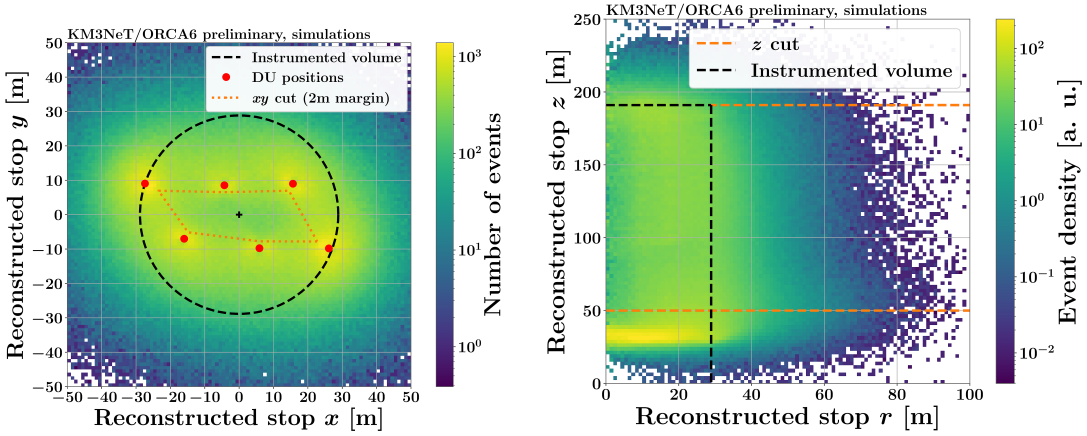

(a) Reconstructed stop positions in the horizontal xy plane **(b)** Reconstructed stop positions in the vertical zr plane

Figure 1: Distribution of the reconstructed stop position of all muon tracks reconstructed in ORCA6, showed with the geometrical cuts applied in the simple cuts approach.

Selecting stopping muons is more challenging than simply selecting the reconstructed muon tracks whose end point is inside the instrumented volume. Indeed, the vast majority of the muons seen by the detector do not stop inside the detector volume but keep traveling much further. Those non-stopping, or *passing* muons, represent about 95% of the muons reconstructed by ORCA6. Yet, many of the passing muons tend to have their stopping point reconstructed inside the instrumented volume, close to the DOMs (as seen on Figure 1a and Figure 1b), because the amount of light detected by the PMTs decreases quickly once the muons move away from the DOMs. Thus, a method to efficiently select true stopping muons, and reject the majority of passing muons, must be developed. Due to the abundant statistics, the methods developed to select stopping muons do not require a very high efficiency. The critical point is the purity of the selection. In the wait for an objective statistical criteria, which will come from further physics analysis, a purity close to 95% is judged satisfying for now.

3. Methods for selecting stopping muons

3.1 Simulation of atmospheric muons

The selection methods were developped using simulated atmospheric muons. The atmospheric muons Monte-Carlo (MC) simulations are done following a run-by-run approach in order to account for the variation of data taking conditions over time. For the generation of the atmospheric muon events at the surface of a virtual cylinder surrounding the active volume of the detector, the MUPAGE package [6] was used, with a parameter tuning specific to KM3NeT [7]. The propagation of generated muons and the PMT response are simulated with a custom KM3NeT software. The output of the simulation chain is a set of digitised PMT output pulses called hits. In addition

to atmospheric muons, around 10% of the events in the data are noise events caused by random coincident hits on the PMTs. They mostly come from the decay of Potassium-40 in the sea water, and are simulated based on the coincidence rate in the data. Finally, the simulated events can be reconstructed under the track hypothesis with the same algorithms used for events in data.

3.2 Selection with simple cuts

The first approach to select stopping muons is to apply a set of cuts on chosen variables with a high separating power between stopping and passing muons. This is called the simple cuts (SC) approach. The cuts and their motivations can be summarized as follows:

- **Energy loss**: stopping muons are minimum ionizing particles (MIP), loosing energy only through ionization loss at a well-defined rate of around 0.25 GeV/m [8]. A cut on the ratio between the reconstructed energy and reconstructed track length is thus applied to remove muons which exhibit higher energy loss rates.
- **Quality of track reconstruction**: it is estimated through the likelihood resulting from the track fitting algorithms. To make that estimation independent of the length of the track, a useful variable is the normalized likelihood, obtained by dividing the likelihood by the number of hits used in the fit. As stopping muons have the end of their track contained in the instrumented volume, we expect the track reconstruction to be of good quality.
- **Number of hits**: As stopping muons have the end of their track contained in the instrumented volume, the number of hits they create on the PMTs should be higher than some threshold.
- **Reconstructed stopping point position**: the reconstructed stopping point should be inside the instrumented volume. But as many passing muons get reconstructed as stopping next to the DOMs, especially near the lowest DOMs (atmospheric muons are downgoing), the reconstructed stopping point is required to be found in an inner region of the instrumented volume. In the horizontal xy plane the boundaries of this fiducial volume are 2 m from the polygon formed by the DU positions, as illustrated in Figure 1a . Along the vertical z axis, to remove all the passing muons reconstructed as stopping near the lowest DOMs (at $z \approx 30$ m) only the stopping points reconstructed above $z = 50$ m are considered.
- **Zenith angle** θ: only muons close to the vertical ($\cos(\theta) < -0.8$) are kept. This is because vertical muons have a longer track in the detector (due to the narrow geometry of ORCA6), making it easier to distinguish between passing and stopping muons.

With this set of cuts, the obtained performances are a **purity of 93%**[1] and an **efficiency of 5%**[2]. Although purity is satisfactory, these cuts (and the geometry of the detector) remove many true stopping muons, preventing access to stopping muons coming with a zenith angle greater than 37° ($\arccos(-0.8)$) from the vertical.

[1]The *purity* of the selection is defined as the percentage of true stopping muons among all those passing the cuts. In literature, this is sometimes referred to as the *precision* or *positive predictive value* $PPV = \frac{TP}{TP+FP}$ where TP are true positive and FP false positive.

[2]The *efficiency* of the selections is defined as the percentage of true stopping muons that get selected among all the true stopping muons reconstructed by the detector. In literature, this is sometimes referred to as the *sensitivity*, the *recall*, or *true positive rate* $TPR = \frac{TP}{TP+FN}$ where FN are false negative.

3.3 Classification with a neural network

To improve efficiency and purity of the stopping muons selection, an approach based on machine learning was developed. A simple neural network (Multi-Layer Perceptron) was trained to classify muons as *stopping* or *passing*. The model which is currently used has 3 layers of 256, 128 and 64 neurons respectively. This makes a total of 48,450 trainable parameters. The input features used by the model come from the track reconstruction algorithms and no individual hit information is used, only summary information on the number of hits. 3 million simulated events were used to train the network, 750,000 to validate it during training, and 1 million to test it after training. To evaluate the dependency of the model on the training and testing sample, a 5-fold cross-validation was performed, showing very limited sample-dependency due to the sufficient sample size.

The model's output is a prediction for the muon's class under the form of a score between 0 and 1. For training, a score of 0 is associated to passing muons and a score of 1 to stopping muons. From that output score distribution, a stopping muon selection can be defined by choosing a cut value on the output score and keeping only the events with a higher score. All the possible purity and efficiency resulting from such a selection, with any chosen cut score value between 0 and 1, is shown on the precision-recall curve Figure 2. In the following, a cut value of 0.85 was chosen, as it allows to reach a **purity of 94%**. The resulting selection also reaches an **efficiency of 25%**. Thus, the machine learning approach offers the possibility to increase the efficiency by a factor 5 with respect to the simple cuts selection, while simultaneously increasing a bit the purity. Most importantly, the ML classification approach allows to access the full zenith angle range while the simple cuts selection was limited to vertical muons.

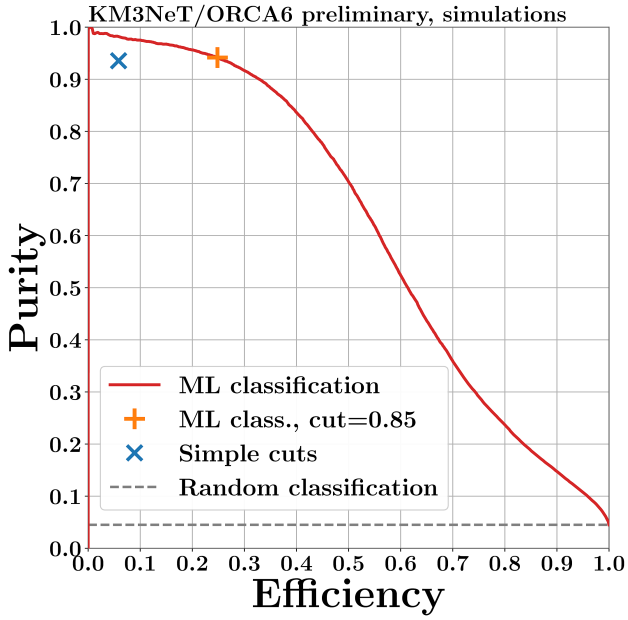

Figure 2: Precision-Recall curve of the machine learning classification. The performances of the two selections (ML classification with the specific cut value chosen and simple cuts) are also shown.

3.4 Comparison of the two selections

Figure 3 shows the comparison of purity and efficiency obtained using the two selections described previsouly as a function of the reconstructed zenith angle and the z coordinate (the height with respect to the seabed) of the reconstructed stopping point. Figure 3b shows that the purity and efficiency of the two selections are close to being constant through most of the detector's height, with a loss of performance at the upper and lower limits of the instrumented volume. Figure 3a shows that the ML classification's selection efficiency decreases with the zenith angle. A possible explanation is that due to the narrow geometry of ORCA6, muons with more horizontal trajectories tend to cross a smaller portion of the instrumented volume. The simple cuts selection sees its purity quickly worsening for non-vertical muons, hence the cut at $\cos(\theta) = -0.8$.

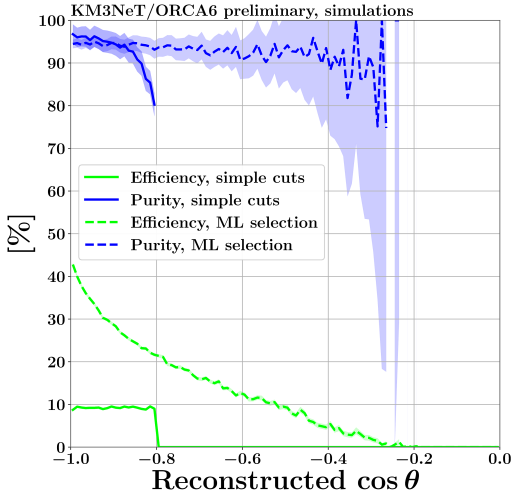

(a) Selection performances as a function of the reconstructed zenith angle

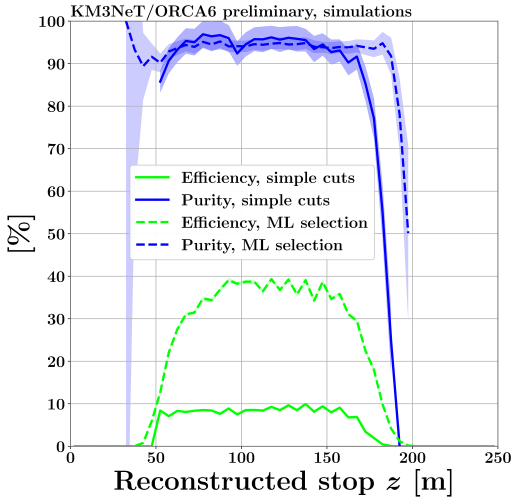

(b) Selection performances as a function of the z-coordinate of the reconstructed stopping point

Figure 3: Performance comparison between the simple cuts and machine learning-based selections.

4. Resolution

Variable	Median value	
	Simple cuts	ML classification
Angular deviation [°]	0.81	1.09
$\Delta SP_{true/reco}$, total [m]	3.9	4.9
$\Delta SP_{true/reco}$, perpendicular to track direction [m]	0.5	0.7
$\Delta SP_{true/reco}$, parallel to track direction [m]	+3.8	+4.6

Table 1: Median resolution values for both selections.

From selected stopping muons, the reconstruction performances of ORCA6 can be evaluated by looking at the error on the reconstructed stopping point and on the reconstructed direction. The very accurate reconstruction capabilities of ORCA6 should be highlighted: the median angular deviation

on the reconstructed tracks is around 1° and the median error on the reconstructed stopping point is less than 5 meters, for both stopping muon selection methods. Table 1 shows more detailed numerical information. In this table $\Delta SP_{true/reco}$ refers to the error made on the reconstruction of the stopping point, overall or projected in the reference coordinate system of the track.

The plus signs in last line of Table 1 mean that the muon tracks tend to be reconstructed as stopping too early along the track direction. In other words, the track reconstruction algorithms miss the last 4 to 5 meters of the tracks in median. Still, it should be highlighted that these resolution values are small compared to the spacing between DOMs (9 m in the vertical direction and 20 m in the horizontal direction). Additionally, studies using stopping muons to determine the atmospheric muons flux at sea level are ongoing. In that context, it must be mentionned that the relative uncertainty on the distance a stopping muon has traveled in the sea water coming from the misreconstruction of track direction and stopping point is negligible (0.1% to 1%).

5. Data-MC comparison

Figure 4a shows the resulting zenith angle distribution of stopping muons from applying both selections on both MC simulations and data, for a livetime of 32.1 days (runs randomly selected over the ORCA6 operating period). The distribution of all reconstructed events, without selection, is also shown for reference. The data/MC ratio for stopping muons is very close to 1.0 overall (0.99 for simple cuts, 0.97 for ML classification) and stable over most of the phase space. Figure 4b also shows that the ratio is 1 through most of the detector's height. This excellent agreement validates the stopping muons selections, as well as the simulations.

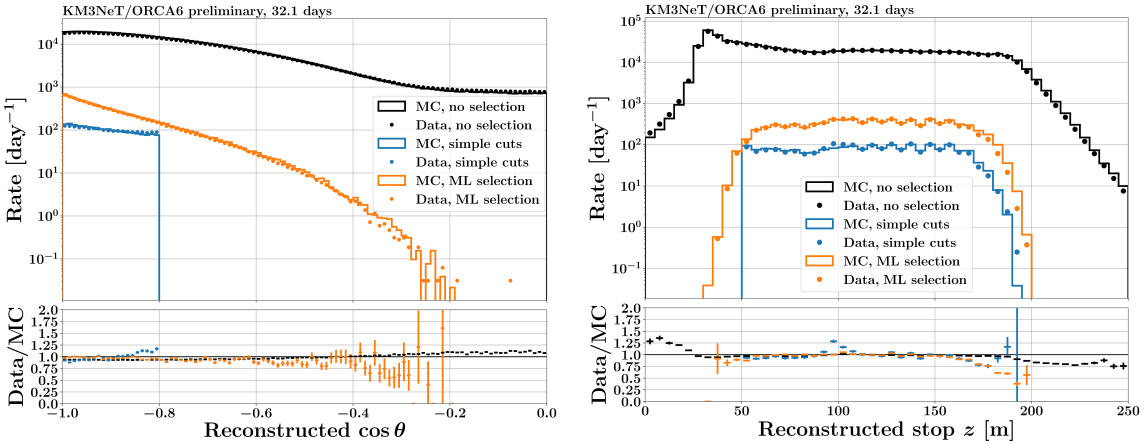

(a) Zenith angle distribution

(b) Stopping point altitude distribution

Figure 4: Data/MC comparison for all muons and for the stopping muons selected with both methods.

6. Conclusion

Two methods for selecting the muons stopping inside the instrumented volume of the KM3NeT/ORCA detector with 6 detection units have been developed. The machine learning-based method allows to select five times more stopping muons than the simple cuts method with very low levels of contamination from passing muons. It also gives acces to the full range of zenith angle.

A study on the angular resolution of the selected stopping muons confirms the very good direction reconstruction capabilities of ORCA, with a median angular deviation of 1°, and shows that the median error on the reconstructed stopping point is less than 5 meters.

A very good agreement between data and simulations can be reached using both stopping muons selections, validating at the same time the selection methods and the simulations.

This preliminary study paves the way for further use of stopping muons. It must be highlighted that the results presented here were obtained with a detector made of 6 detection units only. Future configurations of ORCA, with more DUs, and a more circular footprint, will improve the resolution and the performances of the stopping muon selection methods. Work is already ongoing to use stopping muons to measure the flux of atmospheric muons at sea level on a given range of energy and zenith angle (above 1 TeV for vertical downgoing muons). Another ongoing study measures the subsequent decay of stopping muons.

References

[1] S. Adrián-Martínez et al. (KM3NeT Collaboration), Letter of intent for KM3NeT 2.0, *J. Phys. G*, 43 (2016) 084001.

[2] S. Aiello et al. (KM3NeT Collaboration), The KM3NeT multi-PMT optical module, *J. Inst.*, 17 (2022) 07038.

[3] M. Ageron et al. (KM3NeT Collaboration), Dependence of atmospheric muon flux on seawater depth measured with the first KM3NeT detection units, *Eur. Phys. J. C*, 80 (2020) 99.

[4] A. Fedynitch, F. Riehn, R. Engel, T. Gaisser, T. Stanev, Hadronic interaction model sibyll 2.3 c and inclusive lepton fluxes, *Phys. Rev. D*, 100 (2019) 103018.

[5] R. D. Parsons, H. Schoorlemmer, Systematic differences due to high energy hadronic interaction models in air shower simulations in the 100 GeV-100 TeV range, *Phys. Rev. D*, 100 (2019) 023010.

[6] G. Carminati, M. Bazzotti, A. Margiotta, M. Spurio, Atmospheric MUons from PArametric formulas: A fast GEnerator for neutrino telescopes (MUPAGE), *Comp. Phys. Comm.*, 179 (2008) 915.

[7] B. Ó Fearraigh on behalf of the KM3NeT Collaboration, Tuning parametric models of the atmospheric muon flux in MUPAGE to data from the KM3NeT detector, in *PoSICRC2021* (2021) 1176.

[8] D. E. Groom, N. V. Mokhov, S. I. Striganov, Muon stopping power and range tables 10 MeV–100 TeV, *At. Data Nucl. Data Tables*, 78 (2001) 183.

Full Authors List: The KM3NeT Collaboration

S. Aiello[a], A. Albert[b,bd], S. Alves Garre[c], Z. Aly[d], A. Ambrosone[f,e], F. Ameli[g], M. Andre[h], E. Androutsou[i], M. Anguita[j], L. Aphecetche[k], M. Ardid[l], S. Ardid[l], H. Atmani[m], J. Aublin[n], L. Bailly-Salins[o], Z. Bardačová[q,p], B. Baret[n], A. Bariego-Quintana[c], S. Basegmez du Pree[r], Y. Becherini[n], M. Bendahman[m,n], F. Benfenati[t,s], M. Benhassi[u,e], D. M. Benoit[v], E. Berbee[r], V. Bertin[d], S. Biagi[w], M. Boettcher[x], D. Bonanno[w], J. Boumaaza[m], M. Bouta[y], M. Bouwhuis[r], C. Bozza[z,e], R. M. Bozza[f,e], H.Brânzaş[aa], F. Bretaudeau[k], R. Bruijn[ab,r], J. Brunner[d], R. Bruno[a], E. Buis[ac,r], R. Buompane[u,e], J. Busto[d], B. Caiffi[ad], D. Calvo[c], S. Campion[g,ae], A. Capone[g,ae], F. Carenini[t,s], V. Carretero[c], T. Cartraud[n], P. Castaldi[af,s], V. Cecchini[c], S. Celli[g,ae], L. Cerisy[d], M. Chabab[ag], M. Chadolias[ah], A. Chen[ai], S. Cherubini[aj,w], T. Chiarusi[s], M. Circella[ak], R. Cocimano[w], J. A. B. Coelho[n], A. Coleiro[n], R. Coniglione[w] P. Coyle[d], A. Creusot[n], A. Cruz[al], G. Cuttone[w], R. Dallier[k], Y. Darras[ah], A. De Benedittis[e], B. De Martino[d], V. Decoene[k], R. Del Burgo[e], U. M. Di Cerbo[e], L. S. Di Mauro[w], I. Di Palma[g,ae], A. F. Díaz[j], C. Diaz[j], D. Diego-Tortosa[w], C. Distefano[w], A. Domi[ah], C. Donzaud[n], D. Dornic[d], M. Dörr[am], E. Drakopoulou[i], D. Drouhin[b,bd], R. Dvornický[q], T. Eberl[ah], E. Eckerová[q,p], A. Eddymaoui[m], T. van Eeden[r], M. Eff[n], D. van Eijk[r], I. El Bojaddaini[y], S. El Hedri[n], A. Enzenhöfer[d], G. Ferrara[w], M. D. Filipović[an], F. Filippini[t,s], D. Franciotti[w], L. A. Fusco[z,e], J. Gabriel[ao], S. Gagliardini[g], T. Gal[ah], J. García Méndez[l], A. Garcia Soto[c], C. Gatius Oliver[r], N. Geißelbrecht[ah], H. Ghaddari[y], L. Gialanella[e,u], B. K. Gibson[v], E. Giorgio[w], I. Goos[n], D. Goupilliere[o], S. R. Gozzini[c], R. Gracia[ah], K. Graf[ah], C. Guidi[ap,ad], B. Guillon[o], M. Gutiérrez[aq], H. van Haren[ar], A. Heijboer[r], A. Hekalo[am], L. Hennig[ah], J. J. Hernández-Rey[c], F. Huang[d], W. Idrissi Ibnsalih[e], G. Illuminati[s], C. W. James[al], M. de Jong[as,r], P. de Jong[ab,r], B. J. Jung[r], P. Kalaczyński[at,be], O. Kalekin[ah], U. F. Katz[ah], N. R. Khan Chowdhury[c], A. Khatun[q], G. Kistauri[av,au], C. Kopper[ah], A. Kouchner[aw,n], V. Kulikovskiy[ad], R. Kvatadze[av], M. Labalme[o], R. Lahmann[ah], G. Larosa[w], C. Lastoria[d], A. Lazo[c], S. Le Stum[d], G. Lehaut[o], E. Leonora[a], N. Lessing[c], G. Levi[t,s], M. Lindsey Clark[n], F. Longhitano[a], J. Majumdar[r], L. Malerba[ad], F. Mamedov[p], J. Mańczak[c], A. Manfreda[e], M. Marconi[ap,ad], A. Margiotta[t,s], A. Marinelli[e,f], C. Markou[i], L. Martin[k], J. A. Martínez-Mora[l], F. Marzaioli[u,e], M. Mastrodicasa[ae,g], S. Mastroianni[e], S. Miccichè[w], G. Miele[f,e], P. Migliozzi[e], E. Migneco[w], M. L. Mitsou[e], C. M. Mollo[e], L. Morales-Gallegos[u,e], C. Morley-Wong[al], A. Moussa[y], I. Mozun Mateo[ay,ax], R. Muller[r], M. R. Musone[e,u], M. Musumeci[w], L. Nauta[r], S. Navas[aq], A. Nayerhoda[ak], C. A. Nicolau[g], B. Nkosi[ai], B. Ó Fearraigh[ab,r], V. Oliviero[f,e], A. Orlando[w], E. Oukacha[n], D. Paesani[w], J. Palacios González[c], G. Papalashvili[au], V. Parisi[ap,ad], E.J. Pastor Gomez[c], A. M. Păun[aa], G. E. Păvălaş[aa], S. Peña Martínez[n], M. Perrin-Terrin[d], J. Perronnel[o], V. Pestel[ay], R. Pestes[n], P. Piattelli[w], C. Poirè[z,e], V. Popa[aa], T. Pradier[b], S. Pulvirenti[w], G. Quéméner[o], C. Quiroz[l], U. Rahaman[c], N. Randazzo[a], R. Randriatoamanana[k], S. Razzaque[az], I. C. Rea[e], D. Real[c], S. Reck[ah], G. Riccobene[w], J. Robinson[x], A. Romanov[ap,ad], A. Šaina[c], F. Salesa Greus[c], D. F. E. Samtleben[as,r], A. Sánchez Losa[c,ak], S. Sanfilippo[w], M. Sanguineti[ap,ad], C. Santonastaso[ba,e], D. Santonocito[w], P. Sapienza[w], J. Schnabel[ah], J. Schumann[ah], H. M. Schutte[x], J. Seneca[r], N. Sennan[y], B. Setter[ah], I. Sgura[ak], R. Shanidze[au], Y. Shitov[p], F. Šimkovic[q], A. Simonelli[e], A. Sinopoulou[a], M.V. Smirnov[ah], B. Spisso[e], M. Spurio[t,s], D. Stavropoulos[i], I. Štekl[p], M. Taiuti[ap,ad], Y. Tayalati[m], H. Tedjditi[ad], H. Thiersen[x], I. Tosta e Melo[a,aj], B. Trocmé[n], V. Tsourapis[i], E. Tzamariudaki[i], A. Vacheret[o], V. Valsecchi[w], V. Van Elewyck[aw,n], G. Vannoye[d], G. Vasileiadis[bb], F. Vazquez de Sola[r], C. Verilhac[n], A. Veutro[g,ae], S. Viola[w], D. Vivolo[u,e], J. Wilms[bc], E. de Wolf[ab,r], H. Yepes-Ramirez[l], G. Zarpapis[i], S. Zavatarelli[ad], A. Zegarelli[g,ae], D. Zito[w], J. D. Zornoza[c], J. Zúñiga[c], and N. Zywucka[x].

[a] INFN, Sezione di Catania, Via Santa Sofia 64, Catania, 95123 Italy

[b] Université de Strasbourg, CNRS, IPHC UMR 7178, F-67000 Strasbourg, France

[c] IFIC - Instituto de Física Corpuscular (CSIC - Universitat de València), c/Catedrático José Beltrán, 2, 46980 Paterna, Valencia, Spain

[d] Aix Marseille Univ, CNRS/IN2P3, CPPM, Marseille, France

[e] INFN, Sezione di Napoli, Complesso Universitario di Monte S. Angelo, Via Cintia ed. G, Napoli, 80126 Italy

[f] Università di Napoli "Federico II", Dip. Scienze Fisiche "E. Pancini", Complesso Universitario di Monte S. Angelo, Via Cintia ed. G, Napoli, 80126 Italy

[g] INFN, Sezione di Roma, Piazzale Aldo Moro 2, Roma, 00185 Italy

[h] Universitat Politècnica de Catalunya, Laboratori d'Aplicacions Bioacústiques, Centre Tecnològic de Vilanova i la Geltrú, Avda. Rambla Exposició, s/n, Vilanova i la Geltrú, 08800 Spain

[i] NCSR Demokritos, Institute of Nuclear and Particle Physics, Ag. Paraskevi Attikis, Athens, 15310 Greece

[j] University of Granada, Dept. of Computer Architecture and Technology/CITIC, 18071 Granada, Spain

[k] Subatech, IMT Atlantique, IN2P3-CNRS, Université de Nantes, 4 rue Alfred Kastler - La Chantrerie, Nantes, BP 20722 44307 France

[l] Universitat Politècnica de València, Instituto de Investigación para la Gestión Integrada de las Zonas Costeras, C/ Paranimf, 1, Gandia, 46730 Spain

[m] University Mohammed V in Rabat, Faculty of Sciences, 4 av. Ibn Battouta, B.P. 1014, R.P. 10000 Rabat, Morocco

[n] Université Paris Cité, CNRS, Astroparticule et Cosmologie, F-75013 Paris, France

[o] LPC CAEN, Normandie Univ, ENSICAEN, UNICAEN, CNRS/IN2P3, 6 boulevard Maréchal Juin, Caen, 14050 France

[p] Czech Technical University in Prague, Institute of Experimental and Applied Physics, Husova 240/5, Prague, 110 00 Czech Republic

[q] Comenius University in Bratislava, Department of Nuclear Physics and Biophysics, Mlynska dolina F1, Bratislava, 842 48 Slovak Republic

[r] Nikhef, National Institute for Subatomic Physics, PO Box 41882, Amsterdam, 1009 DB Netherlands

[s] INFN, Sezione di Bologna, v.le C. Berti-Pichat, 6/2, Bologna, 40127 Italy

[t] Università di Bologna, Dipartimento di Fisica e Astronomia, v.le C. Berti-Pichat, 6/2, Bologna, 40127 Italy

[u] Università degli Studi della Campania "Luigi Vanvitelli", Dipartimento di Matematica e Fisica, viale Lincoln 5, Caserta, 81100 Italy

[v] E. A. Milne Centre for Astrophysics, University of Hull, Hull, HU6 7RX, United Kingdom

[w] INFN, Laboratori Nazionali del Sud, Via S. Sofia 62, Catania, 95123 Italy
[x] North-West University, Centre for Space Research, Private Bag X6001, Potchefstroom, 2520 South Africa
[y] University Mohammed I, Faculty of Sciences, BV Mohammed VI, B.P. 717, R.P. 60000 Oujda, Morocco
[z] Università di Salerno e INFN Gruppo Collegato di Salerno, Dipartimento di Fisica, Via Giovanni Paolo II 132, Fisciano, 84084 Italy
[aa] ISS, Atomistilor 409, Măgurele, RO-077125 Romania
[ab] University of Amsterdam, Institute of Physics/IHEF, PO Box 94216, Amsterdam, 1090 GE Netherlands
[ac] TNO, Technical Sciences, PO Box 155, Delft, 2600 AD Netherlands
[ad] INFN, Sezione di Genova, Via Dodecaneso 33, Genova, 16146 Italy
[ae] Università La Sapienza, Dipartimento di Fisica, Piazzale Aldo Moro 2, Roma, 00185 Italy
[af] Università di Bologna, Dipartimento di Ingegneria dell'Energia Elettrica e dell'Informazione "Guglielmo Marconi", Via dell'Università 50, Cesena, 47521 Italia
[ag] Cadi Ayyad University, Physics Department, Faculty of Science Semlalia, Av. My Abdellah, P.O.B. 2390, Marrakech, 40000 Morocco
[ah] Friedrich-Alexander-Universität Erlangen-Nürnberg (FAU), Erlangen Centre for Astroparticle Physics, Nikolaus-Fiebiger-Straße 2, 91058 Erlangen, Germany
[ai] University of the Witwatersrand, School of Physics, Private Bag 3, Johannesburg, Wits 2050 South Africa
[aj] Università di Catania, Dipartimento di Fisica e Astronomia "Ettore Majorana", Via Santa Sofia 64, Catania, 95123 Italy
[ak] INFN, Sezione di Bari, via Orabona, 4, Bari, 70125 Italy
[al] International Centre for Radio Astronomy Research, Curtin University, Bentley, WA 6102, Australia
[am] University Würzburg, Emil-Fischer-Straße 31, Würzburg, 97074 Germany
[an] Western Sydney University, School of Computing, Engineering and Mathematics, Locked Bag 1797, Penrith, NSW 2751 Australia
[ao] IN2P3, LPC, Campus des Cézeaux 24, avenue des Landais BP 80026, Aubière Cedex, 63171 France
[ap] Università di Genova, Via Dodecaneso 33, Genova, 16146 Italy
[aq] University of Granada, Dpto. de Física Teórica y del Cosmos & C.A.F.P.E., 18071 Granada, Spain
[ar] NIOZ (Royal Netherlands Institute for Sea Research), PO Box 59, Den Burg, Texel, 1790 AB, the Netherlands
[as] Leiden University, Leiden Institute of Physics, PO Box 9504, Leiden, 2300 RA Netherlands
[at] National Centre for Nuclear Research, 02-093 Warsaw, Poland
[au] Tbilisi State University, Department of Physics, 3, Chavchavadze Ave., Tbilisi, 0179 Georgia
[av] The University of Georgia, Institute of Physics, Kostava str. 77, Tbilisi, 0171 Georgia
[aw] Institut Universitaire de France, 1 rue Descartes, Paris, 75005 France
[ax] IN2P3, 3, Rue Michel-Ange, Paris 16, 75794 France
[ay] LPC, Campus des Cézeaux 24, avenue des Landais BP 80026, Aubière Cedex, 63171 France
[az] University of Johannesburg, Department Physics, PO Box 524, Auckland Park, 2006 South Africa
[ba] Università degli Studi della Campania "Luigi Vanvitelli", CAPACITY, Laboratorio CIRCE - Dip. Di Matematica e Fisica - Viale Carlo III di Borbone 153, San Nicola La Strada, 81020 Italy
[bb] Laboratoire Univers et Particules de Montpellier, Place Eugène Bataillon - CC 72, Montpellier Cédex 05, 34095 France
[bc] Friedrich-Alexander-Universität Erlangen-Nürnberg (FAU), Remeis Sternwarte, Sternwartstraße 7, 96049 Bamberg, Germany
[bd] Université de Haute Alsace, rue des Frères Lumière, 68093 Mulhouse Cedex, France
[be] AstroCeNT, Nicolaus Copernicus Astronomical Center, Polish Academy of Sciences, Rektorska 4, Warsaw, 00-614 Poland

Acknowledgements

The authors acknowledge the financial support of the funding agencies: Agence Nationale de la Recherche (contract ANR-15-CE31-0020), Centre National de la Recherche Scientifique (CNRS), Commission Européenne (FEDER fund and Marie Curie Program), LabEx UnivEarthS (ANR-10-LABX-0023 and ANR-18-IDEX-0001), Paris Île-de-France Region, France; Shota Rustaveli National Science Foundation of Georgia (SRNSFG, FR-22-13708), Georgia; The General Secretariat of Research and Innovation (GSRI), Greece Istituto Nazionale di Fisica Nucleare (INFN), Ministero dell'Università e della Ricerca (MIUR), PRIN 2017 program (Grant NAT-NET 2017W4HA7S) Italy; Ministry of Higher Education, Scientific Research and Innovation, Morocco, and the Arab Fund for Economic and Social Development, Kuwait; Nederlandse organisatie voor Wetenschappelijk Onderzoek (NWO), the Netherlands; The National Science Centre, Poland (2021/41/N/ST2/01177); The grant "AstroCeNT: Particle Astrophysics Science and Technology Centre", carried out within the International Research Agendas programme of the Foundation for Polish Science financed by the European Union under the European Regional Development Fund; National Authority for Scientific Research (ANCS), Romania; Grants PID2021-124591NB-C41, -C42, -C43 funded by MCIN/AEI/ 10.13039/501100011033 and, as appropriate, by "ERDF A way of making Europe", by the "European Union" or by the "European Union NextGenerationEU/PRTR", Programa de Planes Complementarios I+D+I (refs. ASFAE/2022/023, ASFAE/2022/014), Programa Prometeo (PROMETEO/2020/019) and GenT (refs. CIDEGENT/2018/034, /2019/043, /2020/049. /2021/23) of the Generalitat Valenciana, Junta de Andalucía (ref. SOMM17/6104/UGR, P18-FR-5057), EU: MSC program (ref. 101025085), Programa María Zambrano (Spanish Ministry of Universities, funded by the European Union, NextGenerationEU), Spain; The European Union's Horizon 2020 Research and Innovation Programme (ChETEC-INFRA - Project no. 101008324).